Journal of Materials Processing Technology 209 (2009) 5545–5551

Contents lists available at ScienceDirect

Journal of Materials Processing Technology

journal homepage: www.elsevier.com/locate/jmatprotec

Influence of nodule count on residual stresses and distortion in thin wall ductile iron plates of different matrices

A.D. Sosa[a,b,*], M.D. Echeverría[a], O.J. Moncada[a,b], N. Míngolo[c], J.A. Sikora[b]

[a] Mechanical Technology Group, Universidad Nacional de Mar del Plata, Mar del Plata, Argentina
[b] Metallurgy Division, INTEMA – CONICET, J.B. Justo 4302, (B7608FDQ), Mar del Plata, Argentina
[c] Comisión Nacional de Energía Atómica – UAM – CAC, Buenos Aires, Argentina

ARTICLE INFO

Article history:
Received 19 April 2008
Received in revised form 5 May 2009
Accepted 8 May 2009

Keywords:
Thin wall ductile iron
Nodule count
Austempering
Residual stresses
Distortion

ABSTRACT

Surface characteristics of thin wall ductile iron (TWDI) parts, such as residual stresses, distortion and dimensional changes produced during casting and heat treatment, are relevant variables when it comes to production processes design.

This work focuses on the effect of nodule count on residual stresses (RS) and of TWDI plates distortion. As-cast, ferritised and austempered samples were employed. The role played by two typical austempering temperatures (280 and 360 °C) and three significantly different nodule counts (265, 1200 and 1700 nodules (nod)/mm^2) are discussed by establishing microstructural changes, i.e., microstructure fineness, retained austenite volume fraction (V_γ%), and austenite carbon content (C_γ%). Besides, residual stresses profiles below the surface and dimensional changes are determined.

Results show that all samples display compressive RS on the surface and neighbouring layers. Samples with high nodule count austempered at 280 °C lead to higher compressive RS and distortion as well as to an increase in the RS field below the surface. As-cast and ferritised plates exhibit noticeably lower compressive RS values.

1. Introduction

Ductile irons (DI) are a family of cast alloys that cover a wide range of mechanical properties. They are used to replace successfully cast and forged steels in a large number of applications, thereby providing technical and economic advantages. Therefore, the production of DI has shown a sustained growth rate over the last four decades. Currently, DI producers continue to seek new applications. In particular, recent efforts have aimed to introduce DI parts in the light parts market. Design engineers, vehicle makers and foundrymen are among those industrial community members who are more pressed to produce lighter, stronger, stiffer and cheaper metal parts.

DI is not a light metallic alloy, but it is suited to produce relatively cheap cast parts of complex shape and able to reach very high strength through heat treatments (e.g. austempering). In fact, most DI types have strength to density and elastic modulus to density ratios similar to those of cast aluminium, making it possible to apply DI to light parts. Nevertheless, to make full use of these DI comparative advantages, the parts should have thin walls. Currently, the development of thin wall ductile iron (TWDI) components (parts less than 5 mm thick) is an interesting technological and scientific issue.

Javaid et al. (1989) studied the effect of chemistry and molten metal processing variables on mechanical properties of TWDI. Stefanescu et al. (2003) did research work on mould design and casting process parameters to obtain carbide-free TWDI. Dogan et al. (2003) reported that the greater cooling rate of TWDI parts, when compared to conventional thickness parts, leads to a substantial nodule count increase and to a solidification structure refinement. Massone et al. (2003) studied the kinetics of the solid state transformation of TWDI and concluded that solid state transformation involving carbon transport shows faster kinetics as the nodule count increases; consequently, the mechanical properties of TWDI samples are different from those of regular nodule count, as it has also been demonstrated by David et al. (2004). Dix et al. (2003) agree with those results and also demonstrated that surface roughness influences the level of mechanical properties.

On the other hand, most casting, heat treatment, manufacturing and finishing processes lead to residual stresses (RS) and hardening of metallic materials. RS can reach high values on the surface, and therefore, their mechanical properties and mechanical assembly performance can get noticeably affected. As regards toughness and fatigue strength, they could be improved with high compressive RS.

* Corresponding author at: Metallurgy Division, INTEMA – CONICET, J.B. Justo 4302, (B7608FDQ), Mar del Plata, Argentina. Tel.: +54 223 4816600x260; fax: +54 223 4810046.
E-mail address: adsosa@fi.mdp.edu.ar (A.D. Sosa).

0924-0136/$ – see front matter © 2009 Elsevier B.V. All rights reserved.
doi:10.1016/j.jmatprotec.2009.05.010

Tensile RS may cause stress corrosion cracking in parts subjected to corrosive environments. Besides, an imbalance of the internal stresses associated with RS results in distortion.

Distortion can be significantly increased in the case of thin wall parts and translate into time loss and higher production costs for requiring further machining, stress relief, etc.

RS in heat treated parts can be induced by non-uniform plastic deformations taking place during phase transformations in the cooling step. RS amount and sign are dependent on the resulting microstructures, on temperature gradient and on the part shape and size. Lindgren and Lepistö (2004) noted that RS quantification in heterogeneous materials, characterised by having microstructures composed of two or more phases, calls for a specific analysis, which contemplates the volume fraction relationship of the present phases. This is the case of austempered ductile iron (ADI).

The austempering process to obtain ADI involves an austenitising stage followed by a holding step at constant temperature in a salt bath (typically in the range of 280–360 °C). Subsequently, the austenite is turned into a mix of acicular ferrite and carbon enriched austenite (usually called "ausferrite"). The as-cast microstructure as well as the temperature and holding time of each thermal cycle affect the austenite carbon content and the volume fraction and morphology of the resulting phases. Therefore, mechanical properties can vary within a wide range as it is shown in several tables and figures in Warda (1990).

The austempering of conventional sized DI parts is responsible for shape and dimensional changes (DC) as well as for RS and surface hardening. These effects influence surface properties and likewise later processes such as finish machining, surface treatments and coatings. Sosa et al. (2004) studied RS, distortion and DC on ADI gears. Its effects on performance and loading capacity was analysed by Sosa et al. (2005). The studies carried out by Moncada and Sikora (1996) have demonstrated that DC of conventional sized ADI parts mainly depend on heat treatment parameters and prior microstructure. Echeverría et al. (2001) agree with this results working on ADI parts of thickness ranging from 10 to 40 mm. Nevertheless, to the best of the authors' knowledge RS, DC, distortion and surface hardening have not been reported for ADI parts of small thickness.

The present work aims to determine RS and distortion of TWDI plates with significantly different nodule counts and several matrices in order to obtain useful experimental data for production processes.

2. Experimental procedure

2.1. Materials

A ductile iron melt was produced in a 55 kg medium-frequency induction furnace. Steel scrap and foundry returns were used as raw materials. Nodulisation was carried out using the sandwich method, adding 1.5 Wt% of Fe–Si–Mg (6% Mg). The melt was inoculated with 0.6 Wt% Fe–Si (75% Si) in a separate ladle. Several 2 and 4 mm thick plates and also 25.4 mm Y blocks (ASTM A395) were cast in sand moulds in order to obtain three significantly different nodule counts: 1700, 1200, and 265 nodules (nod)/mm^2, respectively. In all cases nodularity was between 90% and 95% (ASTM A247). Digital image analysis was employed to determine nodule count.

The chemical composition of the melt (Wt%) was as follows: C = 3.40; Si = 3.08; Mn = 0.14; Cu = 0.63; Ni = 0.50; S = 0.013; P = 0.03; Mg = 0.044. It was determined by spark optical emission spectrometry. The carbon equivalent was slightly hypereutectic (CE = 4.43).

2.2. Samples

Sample shape is schematically shown in Fig. 1. "Y" blocks and plates were cut and squared off to dimensions of 100 mm × 13 mm.

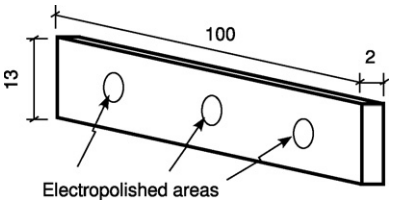

Fig. 1. Test sample scheme. Dimensions in [mm].

Afterwards they were machined by mechanical shaping until reaching 2 mm in thickness. Low-energy cutting conditions were applied to minimise RS generation. Finally, samples were manually polished up to 400 grit with SiC.

A total amount of 72 samples were employed to prepare four batches with different microstructures. Each batch was composed by 18 samples (six samples of each one of the three nodule counts), as described in Section 2.3 and Table 1.

2.3. Heat treatment

Batches were prepared as follows: One batch was employed in the as-cast condition. The other three batches were austenitised at 910 °C for 60 min. After that, two of them were austempered in a salt bath for 45 min, at 280 and 360 °C, respectively. The third batch was kept in the furnace until cooling down to room temperature to obtain a fully ferritic matrix. To avoid decarburisation, samples were placed in a heat-resisting box surrounded by a protection powder consisting basically of iron chips, charcoal particles and $BaCO_3$.

Austempering temperatures (T_a) of 280 and 360 °C were used, taking into account that they are currently employed in the industrial practice. These austempering temperatures promote ADI Grades 1400-1100-02 and 900-650-09 (ASTM A897 M06), respectively, which are extensively used in actual parts production and have high wear resistance or high toughness.

Table 1 lists the characteristics of the batches and samples. Microstructures were analysed by optical microscopy on the surface of a transversal cut performed on each sample, after polishing and etching with nital (2%).

2.4. Measurements

Surface RS (macrostresses) measurements were performed on both sides of the plates (Fig. 1) applying an X-ray technique and the $\sin^2\psi$ method (Rigaku-Strainflex equipment) with the assumption of a biaxial stresses state, such as that described by Hauk (1997), when measurement is confined to the surface of polycrystalline samples. RS were computed based on the relative change of a specified $\{h\,k\,l\}$ diffracting plane in the interplanar spacing (strain) with respect to the stress-free state for different ψ tilt angles between a direction perpendicular to the sample surface and the diffracting plane. RS of ADI samples were only measured on the Fe-α phase, since it is the microconstituent with the greatest volume fraction in the ausferritic microstructure.

A Cr Kα (λ = 0.22897 nm) radiation was selected to attain greater accuracy at a high 2θ angle in the analysis of Fe-α $\{2\,1\,1\}$ diffraction peaks. The 2θ angle ranged from 140° to 170°, with a 2θ step of 0.2° and 1 s by step. The Fe-α $\{2\,1\,1\}$ peaks profiles were recorded at tilt angles of ψ = 0°, 10°, 20°, 25° and 30°, respectively. Radiation penetration depth was of about 5 μm and the assumption of biaxial stresses was considered due to the shallow penetration depth of the X-rays employed.

The RS profile below the surface was also obtained. To do so, a 10 to 200 μm successive layer removal was performed by electropolishing. Fig. 1 depicts the small areas subjected to layer removal.

Table 1
Batches and samples characteristics.

Batch	Nodule Count (nod/mm^2)	Hardness [HB]	Matrix microstructure
As-cast	265	223	Pearlitic–ferritic
	1200	255	
	1700	331	
ADI360 (austempered: 360 °C)	265	331	Fully ausferritic
	1200	335	
	1700	370	
ADI280 (austempered: 280 °C)	265	444	Fully ausferritic
	1200	461	
	1700	477	
Ferritised	265	177	Fully ferritic
	1200	184	
	1700	195	

The X-ray diffraction patterns (XRD) corresponding to the different $\{h\,k\,l\}$ reflections in ferrite and austenite phases were measured in ADI samples to estimate the amount of austenite and its carbon content. Graphite-monochromated Co Kα radiation ($\lambda = 0.1789$ nm) was the option of choice for such measurement. The X-ray tube was operated at 40 kV and 30 mA. Three XRD intensity patterns versus 2θ were obtained for each ADI sample, and a scan in the range of 47–62° with a 2θ step of 0.05° and 0.05 s by step was performed. Powder Cell software developed by Kraus and Nolze (1998), for peak profile refinement was applied to analyse the XRD patterns and to obtain peak positions and intensities as well as austenite volume fraction (V_γ%) and its lattice parameter a_γ. Finally, the percent of austenite carbon content (C_γ%) was estimated by applying the equation taken from Culity (1974):

$$a_\gamma = 3.555 + 0.044C_\gamma\%$$

The percentage variations of other phases, such as non-retained austenite and/or carbides, were disregarded as they are believed not to affect V_γ% and C_γ% estimations.

Likewise, shape distortion was assessed by measurements taken on 20 points of an 80 mm × 10.5 mm rectangular grill after heat treatment. A coordinate measuring machine with an uncertainty of ±(4 + L/1000) μm was employed to that end. Amplified three-dimensional graphs were produced to determine the type and orientation of each specimen distortion. The deflection (δ), or maximum deviation in a perpendicular direction with respect to an ideal plane, was established.

The dimensional change (DC) value of each specimen thickness was determined. Thickness measurements were taken before (Xo) and after (Xf) heat treatment, using a millesimal micrometer with an accuracy of ±(1 + L/75) μm. DC values were calculated as DC = Xf − Xo, and their dispersion was expressed as the standard deviation (ΔDC).

Microhardness profiles were obtained on polished cuts transversal to the surface. For each sample, six micro-Vickers hardness tests were performed under a 0.50N load every 10–25 μm from the surface and along thickness.

3. Results and discussion

3.1. Residual stresses

Fig. 2 lists the average values of surface RS measured on both plate sides for all the studied samples.

All RS are compressive and they increase with microstructure hardness (Table 1). As shown in Fig. 2, the values of RS dispersion are low for ferritic matrices and considerably higher for ADI microstructures.

3.1.1. Nodule count effect

The individual influence of nodule count on RS was only analysed on the ferritised samples, considering the greater matrix homogeneity if compared to that of other microstructures (Table 1). RS increase with nodule count is ascribed to the greater microstructure refinement and to its higher hardness values (Table 1). Caldera et al. (2007) reported that an increase in nodule count promotes an increase in the endurance limit and the fatigue strength for ferritised TWDI samples. Rebasa et al. (2002) found that the rolling contact fatigue life of ferritic samples is longer when the nodule count increases. These results are consistent with the greater compressive RS in samples with the highest nodule count herein reported.

RS dispersion values increase slightly as nodule count decreases (Fig. 2). This is attributed to the greater microstresses heterogeneity resulting from: (i) a larger initial nodule size and (ii) an increase in the graphitic expansion produced by secondary graphite precipitation on the nodules due to carbon migration from the matrix during the ferritising treatment (Fig. 3 shows a layer of secondary graphite precipitated on an original nodule). Section 3.1.2 covers nodule count effect on RS in ADI samples.

3.1.2. Austempering effect

According to the austempering temperature (T_a) and nodule count, ADI samples present different RS values; three times those of the ferritic matrix and twice those of the as-cast one (Fig. 2). Bayati and Elliot (1999) reported differences in thermal properties of DI for different matrix microstructures over temperatures

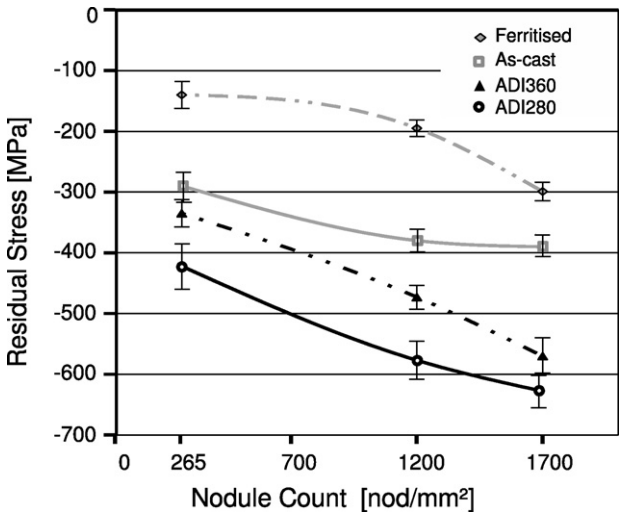

Fig. 2. Surface residual stresses.

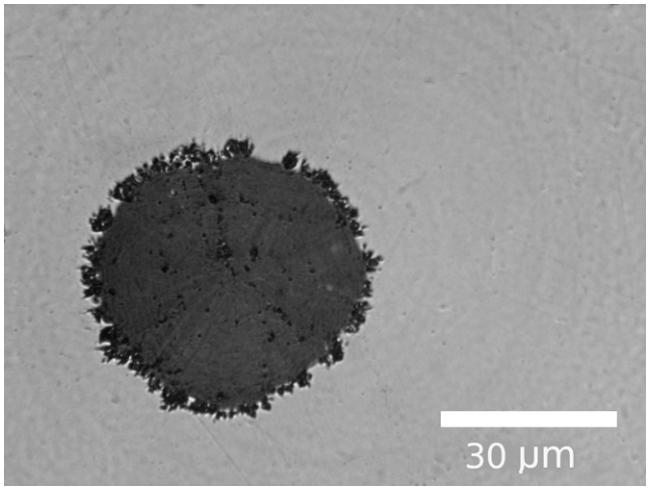

Fig. 3. Secondary graphite layer precipitated on a graphite nodule.

ranging from 200 to 580 °C. Using FEM and experimental methods, Johansson et al. (1999) found that the distribution of phases and the different thermal expansion coefficients affect the macro an microstresses of dual phase steels (austenitic–ferritic). Then, high RS values are attributed to: (i) non-uniform cooling, (ii) changes in lattice parameters due to differences in thermal expansion and mechanical properties between ferrite and austenite, and (iii) to macro–micro RS balance between phases depending on their volume fractions.

RS results and their relationships are analysed for each T_a and nodule count on the basis of the following variables: (a) matrix fineness, (b) volume fraction of the austenite phase (V_γ%), and amount of carbon dissolved in the austenite (C_γ%).

(a) High nodule count plates, austempered at $T_a = 280$ °C, yielded the highest RS values (Fig. 2). During austempering, nucleation and ferrite needles growth processes rely primarily on temperature difference ($T_\gamma - T_a$) as well as on the preferential sites for heterogeneous nucleation provided in the cast microstructure. It can be assumed that low T_a and high nodule counts promote finer ausferritic matrix (see Fig. 4). Coopert et al. (1999) studied the austempering kinetics of DI with nodule counts ranging from 100 to 250 nod/mm^2. Their results agree with those reported by Massone et al. (2003) for TWDI parts. Hence, the smaller ferrite needle size can contribute to increasing microstresses and so RS values. This is consistent with the observations by Lindgren and Lepistö (2003).

(b) V_γ% and C_γ% values turned out to be smaller for $T_a = 280$ °C, as deduced from XRD patterns in Fig. 5a (as example) and Table 2. This can be related to a greater ferrite nucleation rate and to lesser carbon diffusion speed at low austempering temperature.

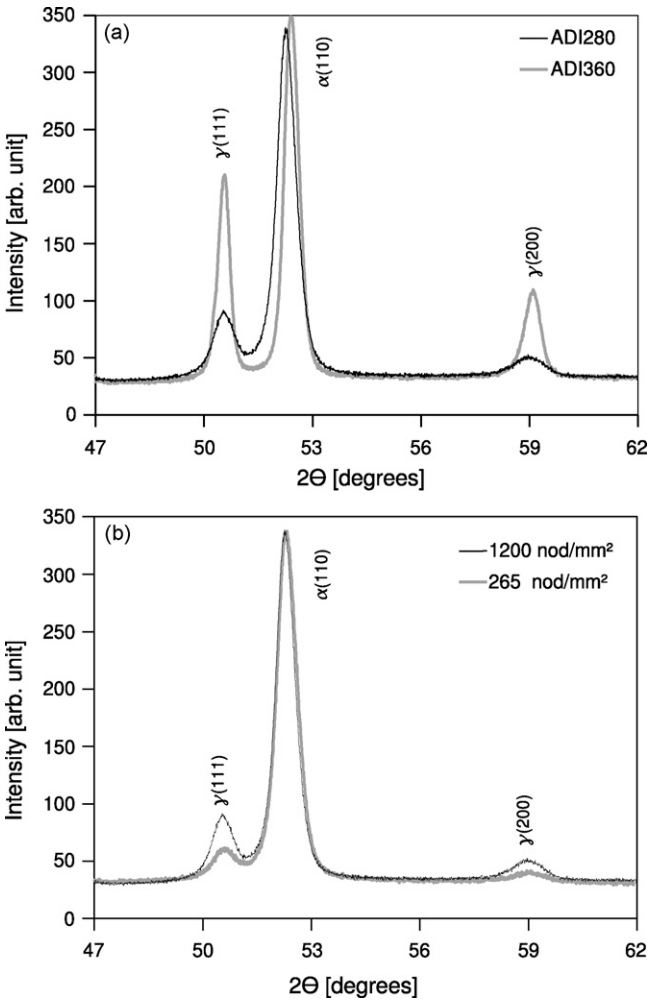

Fig. 5. XRD patterns: (a) Different austempering temperatures (1200 nod/mm^2), (b) Different nodule counts (ADI280).

As it is shown in Fig. 5b (as example) and Table 2, V_γ% increases as the nodule count rises. This is attributed to the increase in the amount of nodule–matrix interface areas and the decrease of internodular distances, which favour carbon diffusion and austenite growth. As it can also be seen in Table 2, the effect of the nodule count is more noticeable for the samples austempered at 280 °C. It can be assumed that the increase in carbon diffusion speed for samples austempered at 360 °C reduces the effect of nodule count on V_γ%. On the other hand, C_γ% variation is not affected by nodule count modification, in agreement with the studies carried out by Massone et al. (2003).

RS analysis and their relationship with T_a, nodule count, and the microstructure features of the ausferritic matrix can be sum-

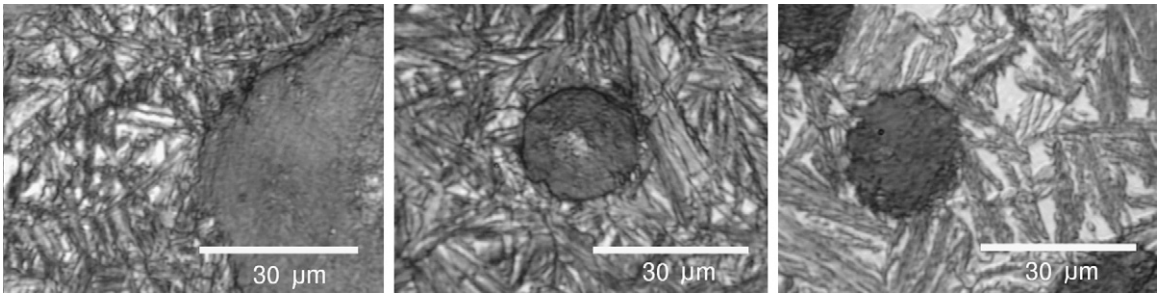

Fig. 4. Ausferritic matrices: (a) ADI280-265 nod/mm^2; (b) ADI280-1200 nod/mm^2; (c) ADI360-1200 nod/mm^2.

marised as follows: RS increase in samples austempered at lower T_a (280 °C), in agreement with the lower V_γ% and C_γ% values, finer microstructure, greater hardness, and higher yield stress. Notwithstanding this, as nodule count increases RS decreases, while V_γ% and C_γ% also diminish. As it is shown in Table 2, V_γ% and C_γ% show little differences when nodule count changes, then the microstructure morphology seems to be the most important variable affecting RS. Thus, high nodule count samples having finer microstructures have higher compressive residual micro and macro stresses. Consequently, improvements in fatigue behaviour and wear resistance are expected in thin wall ADI parts due to the greater compressive RS and hardness, together with an increased V_γ%, taking into account that an increase in nodule count enhances the rolling contact fatigue life, as reported by Dommarco et al. (2006) for different matrix microstructures, including ADI.

3.1.3. RS profile below surface

Fig. 6a–e depict some RS profiles below surface for high and low nodule counts. High compressive RS, which decrease quickly towards the sub-surface layer and become tensile at greater depths,

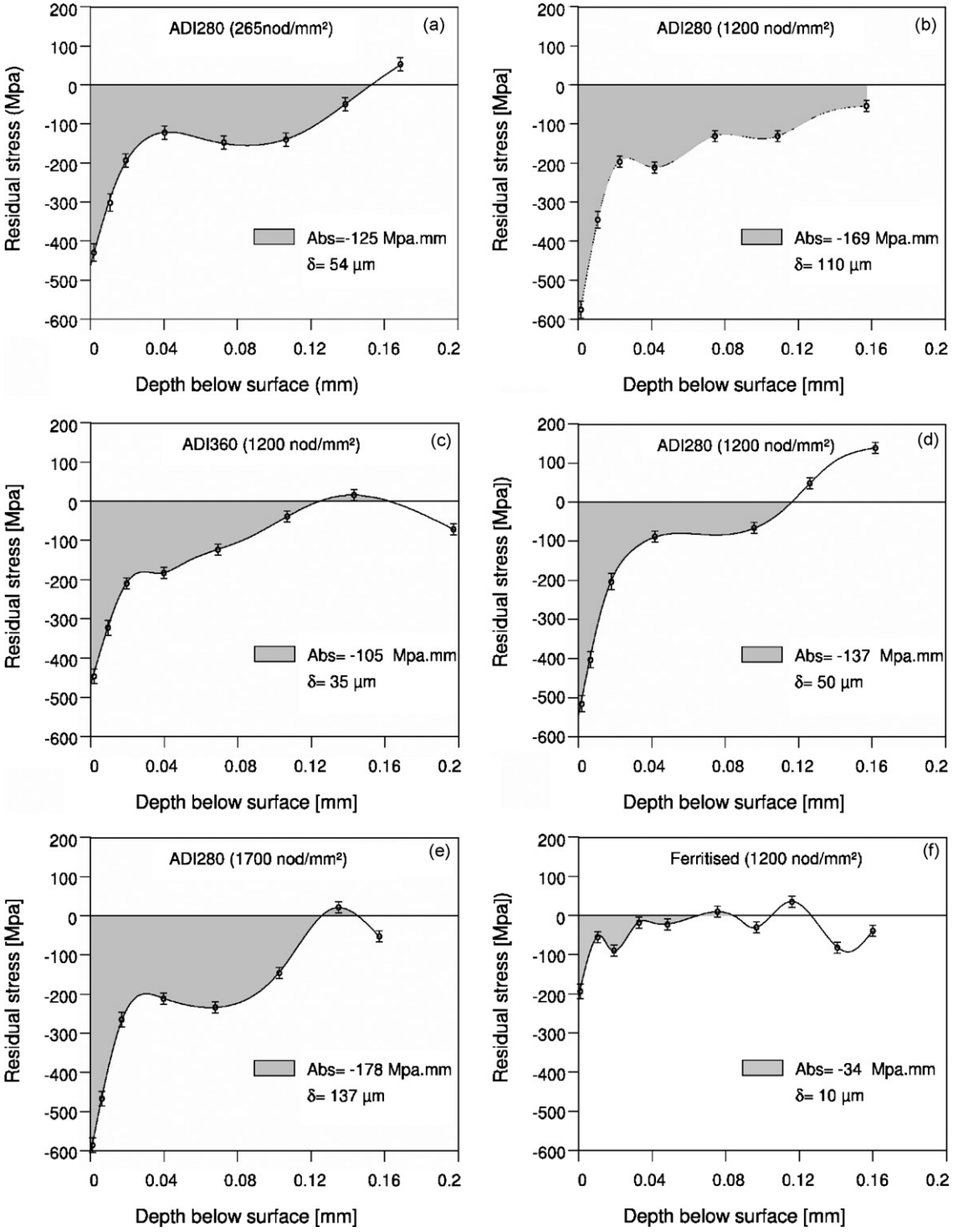

Fig. 6. Representative residual stresses profiles.

Table 2
Austenite volume fractions (V_γ%) and austenite carbon contents (C_γ%).

ADI samples	Nodule count (nod/mm^2)	V_γ%	V_γ increment (%)	C_γ%
ADI280	265	14.2	35.9	1.545
	1200	19.3		1.568
ADI360	265	34.5	12.7	1.727
	1200	38.9		1.727

Table 3
Shape distortion: Deflections δ and dispersion ranges $\Delta\delta$.

	Nodule count (nod/mm^2)	δ (μm)	$\Delta\delta$ (μm)
ADI360	265	23	±10
	1200	51	±30
	1700	55	±25
ADI280	265	65	±19
	1200	108	±46
	1700	115	±56

can be observed. The depths of the compressive RS field as well as their corresponding areas below surface "A_{bs}" expressed in MPa mm, vary in each case. The RS field depth lies in a range of 0.11–0.18 mm. Samples austempered at 280 °C (ADI280) with higher nodule counts present the highest A_{bs} values (Fig. 6e). Similar trends can be noticed between surface RS and A_{bs} areas. Therefore, a more comprehensive analysis of RS profiles and their relationship with shape distortion is carried out in Section 3.2.

Fig. 6f illustrates the RS profile of the ferritised samples exhibiting a smaller compressive field. This can be attributed to the very slow cooling rate (30 ± 5 °C/h) during ferritising in the furnace, from which a more homogeneous matrix of low-energy results.

3.2. Distortion

Shape distortion (or deflection "δ") was detected in samples of all nodule counts austempered at 280 and 360 °C.

Table 3 lists δ average values, and dispersion ranges ($\Delta\delta$). Both variables increase when nodule count increases. For the case of ferritised samples the values of δ and $\Delta\delta$ were neglected.

The distorted samples do not follow a unique shape pattern, but rather feature diverse configurations (either curved or wavy) schematised in Fig. 7a and b. It could be assumed that for ADI280, the comparatively higher cooling rate taking place at the end of the samples with respect to their middle part, accounts for the highest RS variations which provide a "curved" shape. On the other hand, in the case of ADI360 samples, the less severe cooling step results in less distortion, and therefore in a "wavy" configuration.

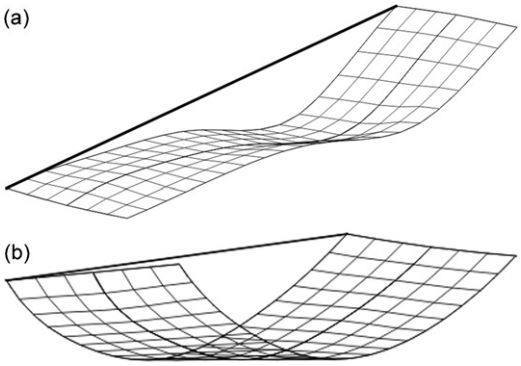

Fig. 7. Schematic representation of distorted shape patterns.

Table 4
Micro-Vickers hardness. Range and average values.

Nodule Count (nod/mm^2)	ADI360		ADI280	
	Range	Average	Range	Average
265	314/342	330	405/428	416
1200	339/355	349	434/463	442
1700	374/390	383	449/478	468

As expected, greater A_{bs} led to greater distortion in ADI280 with the larger nodule count (1700 nod/mm^2). In turn, for each microstructure, the greatest A_{bs} is observed in the test sample with greater distortion δ (Fig. 6) verifying in all cases the overall correlation among RS, A_{bs} and distortion, in agreement with similar trends reported in Dieter (1967) for steels.

It is worth mentioning at this point that the elongated shape and small thickness of the samples play an important role in magnifying δ and $\Delta\delta$. Other factors whose increase influences in a similar way are: (a) the material heterogeneity, and (b) the applied machining energy, whose typical fluctuation results in $\Delta\delta$ increments. Improvements of actual part design together with the implementation of an effective control of the above mentioned factors (a and b) may minimise δ and $\Delta\delta$ avoiding machining operations after heat treatment.

It was found that when nodule count increases and T_a changes from 360 to 280 °C, the dimensional change (DC) of sample thickness also increases, however in no case beyond 8 μm. Dimensional change dispersion (ΔDC) was always below 4 μm. Pursuant to the literature it will be feasible to meet current tolerance manufacturing requirements: T_{IT8} = 14 μm to T_{IT9} = 25 μm (ISO 286-2), by means of reliable machining processes carried out under the most favourable material machinability conditions before heat treatment.

3.3. Microhardness

The hardness of the matrices obtained by austempering proves the well known influence of T_a and reveals the variations introduced by nodule count within the analysed range. The ranges and average micro hardness values of the ausferritic matrices measured on a cut transversal to the surface (excluding the thin external layer (≤10 μm)) is listed in Table 4. It can be seen that when nodule count rises, hardness also increases, which is consistent with the finer microstructure of TWDI parts. It is expected that the combination of high hardness and compressive RS will enhance the wear resistance of thin wall parts (high nodule count). Such favourable results could also be achieved in higher thickness cast parts when nodule count is increased by using special inoculation processes or chills placed in the moulds.

Hardness increase is more significant for T_a = 280 °C and 1700 nod/mm^2, since the combination of a higher undercooling and a higher nodule count contributes to achieving a finer microstructure, and therefore to increase matrix hardness.

As expected, the variation of the matrix hardness with depth is not significant. This is in agreement with the ausferritic microstructure homogeneity due to the small and constant thickness of the samples.

4. Conclusions

Residual stresses (RS) and distortion (δ) of TWDI plates of different matrices are highly affected by nodule count.

Austempered TWDI plates of variable nodule counts show high compressive RS in the surface and neighbouring layers. The maximum depth reached by the RS field approaches

0.2 mm. Ferritic matrices yielded noticeably lower compressive RS.

RS and their compressive field area below surface (A_{bs}) are higher in samples austempered at 280 °C, in comparison with those austempered at 360 °C. This is in accordance with the lower austenite volume fraction (V_γ%) and austenite carbon content (C_γ%), greater hardness and finer microstructure.

High nodule count and finer microstructure promotes the increase of compressive RS. Besides, increase of residual stresses field area below surface (A_{bs}), austenite volume fraction (V_γ%) and hardness, were observed when nodule count increases.

The greatest shape distortion (δ) was found in the case of samples with high nodule count austempered at 280 °C. This is in accordance with the higher values yielded by residual stresses and their field area below surface. On the other hand, ferritised samples showed insignificant distortion.

The shape and the small thickness of the test samples promote high shape distortion. This could be minimised, thereby optimising part design and exerting a thorough control on machining process. In no case did dimensional change exceed 8 μm.

References

Bayati, H., Elliot, R., 1999. Influence of matrix structure on physical properties of an alloyed ductile iron. Mater. Sci. Technol. 15, 265–277.

Coopert, G., Roebuck, A., Bayati, H., Elliot, R., 1999. The influence of nodule count on the austempering kinetics of a Mn–Cu ductile iron. Int. J. Cast Metals Res. 11, 227–235.

Culity, B.D., 1974. Elements of X-ray Diffraction. Addison–Wesley Reading, MA, p. 508.

David, P., Massone, J., Boeri, R., Sikora, J., 2004. Mechanical properties of thin wall ductile iron-influence of carbon and graphite distribution. ISIJ Int. 44 (7), 1180–1187.

Dieter Jr., G.E., 1967. Mechanical Metallurgy. McGraw-Hill Book Company, Inc., New York, pp. 438–446.

Dix, L.P., Ruxanda, R., Torrance, J., Fukumoto, M., Stefanescu, D.M., 2003. Static mechanical properties of ferritic and pearlitic lightweight ductile iron castings. In: AFS Transactions, vol. 111 Proceeding of 107th Annual Casting Congress, 109, Milwaukee, Wisconsin, USA, pp. 1–16.

Dogan, Ö.N., Schrems, K.K., Hawk, J.A., 2003. Microstructure of thin-wall ductile iron castings. In: AFS Transactions, vol. 111 Proceeding of 107th Annual Casting Congress, 136, Milwaukee, Wisconsin, USA, pp. 1–11.

Caldera, M., Chapetti, M., Massone, J.M., Sikora, J.A., 2007. Influence of nodule count on fatigue properties of ferritic thin wall ductile iron. Mater. Sci. Technol. 23, 000–004.

Dommarco, R.C., Jaureguiberry, A.J., Sikora, J.A., 2006. Rolling contact fatigue resistance of ductile iron with different nodule counts and matrix microstructures. Wear 261, 172–179.

Echeverría, M.D., Moncada, O.J., Sikora, J.A., 2001. Influence of the dimensional change, and its dispersion, on the fabrication size tolerances of adi parts: comparison with sae 4140 steel. ISIJ Int. 41, 25–30.

Hauk, V., 1997. Structural and Residual Stress analysis by Nondestructive Methods. Elsevier Science, Amsterdam.

Javaid, A., Davis, K.G., Sahoo, M., 1989. Effect of chemistry and processing variables on mechanical properties of thin-wall di castings. In: AFS Transactions, vol. 89 Proceeding of 93th Annual Casting Congress, San Antonio, Texas, USA, pp. 191–200.

Johansson, J., Oden, M., Zeng, X., 1999. Evolution of the residual stress in a duplex stainless steel during loading. Acta Mater. 47 (9), 2669–2684.

Kraus, W., Nolze, G., 1998. Powder cell 2.3 version. CPD Newslett. 20, 274.

Lindgren, M., Lepistö, T., 2003. Relation between residual stress and Barkhausen noise in a duplex steel. NDT&E Int. 36, 279–288.

Lindgren, M., Lepistö, T., 2004. On the stress vs. Barkhausen noise relation in a duplex stainless steel. NDT&E Int. 37, 403–410.

Massone, J.M., Boeri, R.E., Sikora, J.A., 2003. Solid state transformation kinetics of high nodule count ductile iron. Int. J. Cast Metals Res. 16 (1-3), 179–184.

Moncada, O.J., Sikora, J.A., 1996. Dimensional change in austempered ductile iron. AFS Trans. 109 (96–147), 577–580.

Rebasa, N., Dommarco, R., Sikora, J.A., 2002. Wear resistance of high nodule count ductile iron. Wear 253, 855–861.

Sosa, A.D., Echeverría, M.D., Moncada, O.J., 2004. Machining and heat treatment effects on distortion and residual stresses in an industrial application of adi. ISIJ Int. 44. (7), 1195–1200.

Sosa, A.D., Echeverría, M.D., Moncada, O.J., 2005. Analysis of stresses in ADI internal gears mounted with interference; distortion and residual stresses effects. Lat. Am. Appl. Res. 35, 241–246.

Stefanescu, D.M., Ruxanda, R., Dix, L.P., 2003. The metallurgy and tensile mechanical properties of thin wall spheroidal graphite irons. Int. J. Cast Metals Res. 16 (1-3), 319–324.

Warda, R.D., 1990. Section IV, Austempered ductile iron. In: QIT-Fer et Titane Inc. (Ed.), Ductile Iron Data for Design Engineers. Metrolitho Inc. Press, Canada, pp. 4-1-4-44.